Title

Reversible Crosslinked Polymer Binder for Recyclable Lithium Sulfur Batteries with High Performance

Journal

Advanced Functional Materials, 30(36)

ISSN

1616-301X

Authors

Liu, Zhimeng
He, Xin
Fang, Chen
et al.

Publication Date

2020-09-01

DOI

10.1002/adfm.202003605

Peer reviewed

DOI: 10.1002/afm-journal-S-20-03605
Full Paper

Reversible crosslinked polymer binder for recyclable lithium sulfur batteries with high performance

*Zhimeng Liu[#], Xin He[#], Chen Fang, Luis E. Camacho-Forero, Yangzhi Zhao, Yanbao Fu, Jun Feng, Robert Kostecki, Perla B. Balbuena, Junhua Zhang, Jingxin Lei and Gao Liu**

Z. Liu, Dr. X. He, Dr. C. Fang, Dr. L. E. Camacho-Forero, Dr. Y. Zhao, Dr. Y. Fu, Dr. R. Kostecki, Dr. G. Liu
Energy Storage and Distributed Resources Division, Lawrence Berkeley National Laboratory, Berkeley, California 94720, USA
E-mail: gliu@lbl.gov

Z. Liu, Prof. J. Zhang, Prof. J. Lei
State Key Laboratory of Polymer Materials Engineering, Polymer Research Institute of Sichuan University, Chengdu 610065, China

Dr. L. E. Camacho-Forero, Prof. P. B. Balbuena
Department of Chemical Engineering, Texas A&M University, College Station, Texas 77843, USA

Dr. J. Feng
Advanced Light Source, Lawrence Berkeley National Laboratory, Berkeley, CA 94720, USA

[#] The authors Z. Liu. and X. He. made equal contribution to the work.

Keywords: binder; recyclable; high sulfur loading; lithium sulfur batteries

Abstract

Grappling with diminishing negative impact on environment associated with extensive utilization of batteries, sustainability of the cells needs to be included in systemic research of batteries. Herein, a dissolvable ionic crosslinked polymer (DICP) was exploited as a binder for lithium-sulfur batteries by crosslinking the polyacrylic acid (PAA) and polyethyleneimine (PEI) through carboxy-amino ionic interaction. This interaction is pH-controlled, and

therefore the crosslinked binder network can be readily dissociated in basic condition, providing a facile strategy enabling valuable components recycled through a convenient washing method. The sulfur cathode prepared by the recycled carbon-sulfur composite can deliver comparable capacity as that of fresh electrode. In addition, evidence from cell performance and characterizations, such as in-situ X-ray absorption spectroscopy (XAS), in-situ UV-visible spectroscopy (UV-vis), X-ray photoelectron spectroscopy (XPS) and Density Functional Theory (DFT) calculation, confirms that DICP is a more effective binder than its commercial counterpart on suppressing polysulfide dissolution in the electrolyte. Exploiting reversible crosslinked polymer binder for recyclable Li-S batteries with ameliorated electrochemical performance, this study illuminates sustainable development for large-scale energy storage systems.

1. Introduction

In response to urgent appeal of shrinking urban air pollution from vehicles exhaust, the automotive industry is currently experiencing an energy revolution, with vehicles powered by gasoline transferring to transportations driven by electric power. During this decarbonization advancement, innovation of lithium-ion battery (LIB) technology is pivotal since it plays an indispensable role in using more renewables and providing less expensive batteries while preserving high power density. [1,2] Despite substantial progress that has been made in the performance of LIBs, new challenges, such as shortage and uneven geographic distribution of resources (especially for Co and Li) for cathode synthesis, raw material extraction, and proper management for end-of-life materials, are posed to long-term economic strain as the number of electric vehicles steadily increasing.[3] The recycling of LIBs is a feasible approach to directly address concerns about the resource supply and environmental issues associated with landfilling. However, the widely adopted LIBs recycling process for material extraction

is to fully dissolve the entirely mixed-metal electrode by leaching with reductive acid. A complex leachate is produced, which needs to be separated and purified through involving a series of selective precipitation and/or solvent extraction steps.[4] Therefore, to achieve further environmental soundness accompanying with expansive utilization of electrifications, research attention needs to be paid in exploring the sustainability of batteries, selecting chemistries that have a minimum footmark in nature and that are more easily recycled,[1,5] a process that is pertinent to the development of future circular economy.

Among possible candidates of electrode materials, sulfur stands out as the most promising selection because of various advantages, including its natural abundance, cost-saving, and superior theoretical capacity ((1675 mAh g^{-1})) as well as energy density (2600 Wh kg^{-1}).[6–8] These valuable merits are highly desired for the development of next-generation LIBs. Therefore, Li-S batteries have attracted a great amount of attention in recent years.[9,10] Despite their promising properties, the practical application of Li-S batteries is still limited by the following issues: (1) the dissolution and diffusion of polysulfide intermediates (lithium polysulfide products, Li_2S_n, $4 \leq n \leq 8$) in the electrolyte,[11,12] resulting in the loss of active sulfur on the cathode and a low coulombic efficiency; (2) the poor electron and ionic conductivity of sulfur and sulfides, leading to the low utilization of sulfur and inferior rate capability;[13,14] (3) large volume changes (about 78% of volume variation upon cycling), giving rise to the damage of integrity for the electrode.[15,16] These issues inevitably influence the performance of Li-S batteries, ultimately causing suppressed delivered capacity and fast capacity fading during cycling.[17,18]

Tremendous efforts have been invested to address the issues mentioned above, focusing on the construction of sophisticated cathode architectures. Usually, sulfur materials are infiltrated to conductive carbon hosts with various morphologies and microstructures. It has been reported that several types of carbon hosts, including hollow carbon,[19] porous carbon,[20] disordered carbon nanotubes,[21] mesoporous carbon nanoparticles,[22] double-

shelled hollow carbon spheres,[23] and carbon foam,[24] have made significant enhancement in delivering specific capacity and cycling stability of Li-S batteries. However, the preparation of these complicated carbon materials involves several complicated and energy-intensive steps,[25–27] increasing the thermal budget and carbon footprint. Therefore, to reduce the overall cost considerably, it is imperative to develop facile strategies to recycle the valuable carbon hosts at their end-of-life.

Another efficient strategy improving the electrochemical performance of Li-S batteries is to develop multi-functional binders that are capable of trapping the lithium polysulfides.[10,28–30] As an essential ingredient of electrode composites, the binder is responsible for gluing the active material together with conductive additive on the current collector, and can maintain the integrity of electrode to ensure the electronic and ionic conductivity.[31,32] However, the conventional poly(vinylidene fluoride) (PVdF) binder can only provide quite poor adhesion strength, which is hard to maintain integrity well for sulfur-based cathode due to huge volume variation during the lithiation/delithiation processes, causing the rapid capacity decay.[20,33] Thus, polymers with polar groups to confine the dissolution of lithium polysulfides are urgently desirable. According to the previous reports, the crosslinked polymer with multiple functional groups can effectively mitigate the volume expansion and limit the shuttle of lithium polysulfides and, consequently, significantly improve the performance of Li-S batteries, especially for high sulfur loading.[16,28,34,35] For instance, Yan et al.,[36] synthesized a new binder via co-polymerization of hexamethylene diisocyanate with polyethyleneimine (PEI) to form a network structure with high proportion of amine groups. Moreover, the sulfur loading areal capacity can reach 7.9 mAh cm^{-2}, and the capacity retention is 91.3% over 600 cycles at 2C. Similarly, Nazar's[37] group prepared a stable high sulfur loading cathode by combining multifunctional sulfur composites with an in-situ cross-linked polymer binder, where the carboxymethyl cellulose was polymerized with small citric acid molecules in-situ formed a reticular structure through the dehydration

condensation reaction and, as a consequence, crack-free high sulfur loading electrodes (up to 14.9 mg cm^{-2}) with high areal capacities (up to 14.7 mAh cm^{-2}) and stable cycling life were obtained owing to the elastomeric cross-linked binder. Although the high mass loading and stable cycling sulfur electrode can be achieved by crosslinked polymers, most of them are unable to be dissolved in the solvent once they are polymerized. The valuable electrode materials in these designed electrodes are unable to be recycled through a simple method.

In this work, a facile strategy is employed to recycle carbon-sulfur (C-S) composite materials from cycled electrodes by utilizing a dissolvable ionic crosslinked polymer (named as DICP) binder. The three-dimensional network structure of DICP is formed by crosslinking polyacrylic acid (PAA) and polyethyleneimine (PEI) through carboxy-amino ionic interaction. This interaction is pH-controlled, and therefore, the crosslinking is readily dissociated in basic condition (i.e. aqueous sodium hydroxide or ammonium hydroxide solution), thus providing a plausible approach to recycle valuable electrode materials through a simple washing method based on water. The three-dimensional network structure of DICP significantly enhances the mechanical integrity of C-S composite for high sulfur loading electrodes formation. In addition, confinement of polysulfide intermediate species is realized through the strong affinity interaction with polar functional groups (i.e. amino and ammonium) within the DICP. Therefore, with the application of this robust binder, the Li-S battery could achieve excellent electrochemical performance, obtaining a high sulfur loading electrode of 5.5 mg cm^{-2} with an areal capacity of 6.39 mAh cm^{-2}. The recycled C-S composite could be re-fabricated into sulfur cathodes exhibiting approximately comparable capacity as that of fresh cathodes. To the best of knowledge, this is the first report of a recyclable Li-S batteries. The solvent employed in both the electrode preparation and the recycling processes is merely low-cost distilled water. Providing an eco-efficient perspective for Li-S batteries recycling, this study displays a prospect that is closely germane to green chemistry and circular economy.

1. Results and discussion

The design concept and synthesis schematic of DICP is displayed in Figure 1(a), a three-dimensional network structure of DICP possessing abundant polar functional groups (i.e. amino and ammonium) is constructed by crosslinking PAA and PEI through the carboxy-amino ionic interaction. This interaction is pH-controlled in water, and therefore the crosslinked structure of DICP is easily destroyed and dissolved in basic aqueous solution (i.e. aqueous sodium hydroxide or ammonium hydroxide solution), as shown in Figure 1(b). Upon casting the DICP solution (prepared in ammonium hydroxide solution) in PTFE mold, a transparent DICP film was obtained (Figure 1(c)). After being immersed in distilled water for 12 h, the DICP film turns white only and does not dissolve in water (Figure 1(d)), indicating the formation of a three-dimensional crosslinked network structure in DICP that is stable in distilled water. However, the film is dissolved completely in basic aqueous solution (pH=13) within 1 h, forming a homogeneous solution, indicating that the DICP film can be dissolved in basic aqueous. As shown in Figure 1(f-h), after being immersed in electrolyte for 12 h, the DICP film does not dissolve without displaying any size variation. After being immersed in the electrolyte for 12 hours, the swelling ratio of DICP film is 2.3%, which is much lower than that of PAA (77.1%) and PVDF (18.9%), as shown in Figure S1 (Supporting Information). The results indicate superior stability of DICP in electrolyte.

The chemical structure of DICP was confirmed by Fourier transform infrared (FTIR) spectroscopy and the results are shown in Figure S2 (Supporting Information). The characteristic absorption peaks at 3349 cm^{-1}, 3281 cm^{-1} 1649 cm^{-1} 1592 cm^{-1}, and 1462 cm^{-1} are attributed to the N-H stretching vibration in the spectrum of PEI.[38] The two peaks around at 2940 cm^{-1} and 2822 cm^{-1} correspond to the C-H stretching vibration of -CH_2-CH_2-.[38] A broad absorption band at 3130 cm^{-1} can be observed in the spectrum of PAA, corresponding to the O-H stretching vibration, whereas the strong peak at 1724 cm^{-1} ascribed to the C=O stretching vibration in -COOH.[39] Compared to the spectrum of PEI and PAA, the broad

absorption band at 3130 cm^{-1} for O-H stretching vibration disappears for the DICP sample. The primary N-H stretching vibration of PEI at 3281 cm^{-1} shifted to 3260 cm^{-1}, 1649 cm^{-1} shifted to 1613 cm^{-1}, and C=O stretching vibration of PAA at 1724 cm^{-1} shifted to 1548 cm^{-1}, as the result of the ionic interactions with the formation of carboxylic acid ammonium salt[40] between PAA and PEI.

Figure 2 shows the loop of the electrode preparation and recycling process. The electrodes with sulfur loading around 5.0~6.0 mg cm^{-2} were prepared by using DICP as binder and nickel foam as the current collector, and the coin cells were assembled in Ar filled glove box (experimental details are shown in supporting information). After 100 cycles at 0.1C (1C=1675 mA g^{-1}), the Li-S cells were first disassembled in the glove box to retrieve the cycled sulfur electrodes (Figure 2(b)). Then, the collected electrodes were immersed into aqueous NaOH solution (pH=13) to dissociate the binder network. As shown in Fig 2(c), the electrode materials were dispersed into water under continuous stirring conditions. Afterward, current collectors and mixed solution were separated naturally without further steps. The recycled C-S composite powder (yield:~61%) was obtained (Figure 2(d)) by following washing (with distilled water)-centrifuging-drying (at 50 ℃ for 5h) process. The average particle size of recycled C-S composite is 15.1 μm based on the particle size measurement result (Figure S3, Supporting Information). The amount of residual sulfur in recycled C-S composite was confirmed by thermal gravimetric analysis (TGA). The TGA curve of recycled C-S composite only shows one-step weight loss in the temperature range of 130~300 ºC, corresponding to the loss of sulfur (Figure S4, Supporting Information). The detected weight loss of this step is about 25.7%. Figure S5 (Supporting Information) reveals the TGA curve of pure DICP, indicating the thermal decomposition process of DICP. However, no peaks can be assigned to the thermal decomposition of DICP in the temperature range of 300-450 ℃ in

Figure S4 (Supporting Information), suggesting no residual DICP in the recycled composite. The proper amount of sulfur powder was mixed with recycled C-S composite to compensate for the sulfur loss during battery cycling (70 wt% final sulfur content) for the next round of cycling. In the end, the new sulfur electrode was prepared in the same procedure introduced in the first step.

The top view scanning electron microscope (SEM) images of S@DICP, S@PAA, and S@PVdF electrode are shown in Figure S6 (Supporting Information). The electrode prepared with the DICP binder exhibits a smooth surface, whereas the S@PAA electrode displays a rough surface with fine fissure, and the S@PVdF electrode shows evident cracks in the composite. The better electrode integrity of the S@DICP electrode is contributed by the crosslinked network structure of DICP, which has strong mechanical capability to hold the C-S composite together. The adhesion of binder is also of great benefit to the electrochemical performances of electrodes.[41] Low adhesion leads to the loss of active material and degrades of conductivity, engendering continuous capacity fading and poor cycling stability. To evaluate the adhesion of DICP, peeling tests were conducted. As shown in Figure S7 (Supporting Information), the S@DICP exhibits a superior peeling force, and no obvious material loss can be observed from the S@DICP electrode. By contrast, the whole and a certain amount of electrode material was peeled off from the current collector of S@PVdF and S@PAA electrode, respectively (Figure S8, Supporting Information), suggesting a much weaker adhesion strength of PAA and PVdF than that of DICP.

Electrochemical tests were conducted with the application of DICP, PAA, and PVdF as the binder for Li-S batteries. The electrochemical stability of DICP was first evaluated by cyclic voltammetry (CV). Figure S9 (Supporting Information) demonstrates that the DICP is electrochemically stable in the voltage range from 1.7 to 2.8 V *vs.* Li/Li^+. The CV curves of sulfur electrodes with different binders are shown in Figure 3a. The assembled Li-S cell was

measured under the scanning rate of 0.1 mV s^{-1} in the same voltage range (1.7-2.8 V). Two reduction peaks appear at 2.2-2.4 V and 1.8-2.1 V on the CV curve of S@DICP, S@PAA and S@PVdF electrode assembled Li-S cell, corresponding to the transition of elemental sulfur to long-chain lithium polysulfide (Li_2S_n, $4 \leq n \leq 8$), and further to low-order Li_2S_2/Li_2S, respectively. During the reverse scan of the S@PVdF electrode, there is only one broad oxidation peak at 2.2-2.6 V can be assigned to the reverse transition from Li_2S_2/Li_2S to Li_2S_n ($4 \leq n \leq 8$) and further to elemental sulfur.[36,42] Despite similar redox characteristic peaks, the S@DICP shows a significant reduction in voltage polarization in comparison with S@PVdF. Meanwhile, the CV peaks of S@DICP are much sharper than those of S@PVdF. All the above differences confirm that the S@DICP, with favorable lithiation and delithiation during electrochemical reactions, profoundly enhances the reaction kinetics.[43] As reported previously, the reaction kinetics can be affected by electrical conductivity and polysulfide/Li_2S affinity of host materials.[44] Therefore, it can be concluded that the abundant affinity groups contained by DICP promote the charge transfer and intermolecular binding, accounting for the improved kinetics. With the further cycles of S@DICP (Figure S10, Supporting Information), the reduction peaks shift to the higher voltages, while oxidation peaks shift to the lower potentials, and redox peaks become slightly sharper, demonstrating further decreasing of the polarization, which can be attributed to the strong absorption affinity of DICP towards polysulfides.[42]

The first cycle discharge-charge profile (0.5 C) of S@PVdF, S@PAA, and S@DICP electrodes are shown in Figure 3b. The voltage of discharge plateaus for S@DICP is higher, whereas the charge plateau is lower than that of S@PVdF and S@PAA. It suggests the enhancement of reaction kinetic. Therefore, in the first discharge stage, S@DICP delivers more capacity than that of S@PVdF and S@PAA, testifying that the transition of elemental sulfur to lithium polysulfides is more complete in S@DICP. When cycling at 0.5C, S@DICP gives an initial discharge capacity of 1035 mAh g^{-1}; while the initial discharge capacity of

S@PVdF and S@PAA is 979 mAh g^{-1} and 954 mAh g^{-1}, respectively (shown in Figure 3c). After 200 cycles, the distinction becomes more evident. S@DICP delivers a discharge capacity of 780 mAh g^{-1}. In contrast, much lower capacity can be retained for S@PVdF and S@PAA. In addition to cycling stability at low rate, S@DICP also displays a superior rate performance. With retaining 701 mAh g^{-1} at 3C, discharge capacity exhibits 245 mAh g^{-1} and 518 mAh g^{-1} higher than that of S@PAA and S@PVdF, respectively (Figure 3d). Such a superior cycling stability and high rate capability of S@DICP can be attributed to the chemical structural advantages (crosslinked network structures and a large number of multifunctional polar groups) of DICP that maintain electrode's integrity and confine the lithium polysulfide within the cathode. These chemical structural benefits are more profound in high sulfur loading electrodes. To reach higher energy density than conventional batteries, the mass loading of the sulfur electrode should be above 5.0 mg cm^{-2}.[45] Therefore, sulfur electrodes with mass loading around 5.5 mg cm^{-2} were prepared by using the nickel foam as current collect. As shown in Figure 3e, S@DICP electrode with high initial discharge capacity of 1448 mAh g^{-1} equivalent to the area capacity of 6.39 mAh cm^{-2} is obtained at a current density of 0.05C (0.46 mA cm^{-2}), which is higher than that of S@PAA electrode (1323 mAh g^{-1}) and S@PVdF electrode (1200 mAh g^{-1}). When cycled at 0.1C (0.92 mA cm^{-2}), the S@DICP exhibits quite stable cycling performance. The discharge capacity can still reach to 841.7 mAh g^{-1} after 100 cycles, corresponding to the 3.71 mAh cm^{-2}. By contrast, both S@PAA and S@PVdF cannot run more than 50 cycles even with much lower delivered capacity.

Figure 3(f) shows the performance of the Li-S cell assembled with recycled S@DICP electrode. The delivered discharge capacity and cycling stability are the same as the electrode prepared with pristine sulfur-carbon composite, as demonstrated in Figure 3(e). The electrochemical result confirms that using DICP as binder not only enhances the sulfur

loading and cyclic stability, but also enables successful recycling of sulfur-carbon composite from cycled Li-S cells via an environmentally friendly process.

In order to gain insight into the confining capability of lithium polysulfides by different binders, in-situ X-ray absorption spectroscopy (XAS) experiments were conducted to monitor the concentration variation of lithium polysulfides in electrolyte within coin cell (Figure 4a). XAS spectra are selected when the voltage reaches 2.38 V, 2.23 V, 2.13 V, 2.08 V, and 1.70 V (Star pointed in Figures 4b, c, and d) for S@PVdF, S@DICP and S@PAA electrode, as shown in Figure 4(e-g). The strong peak at 2479.0 is ascribed to the sulfonyl groups in LiTFSI[11,46], and new peaks at 2471.8 eV and 2475.3 eV occurring during the discharge process can be attributed to the formation of neutral sulfur (Li_2S_x and Li_2S), respectively.[47,48] As for S@PVdF and S@PAA electrodes, the signal of Li_2S_x can be first detected when the voltage reaches down to 2.23 V (green star point), indicating the dissolution of Li_2S_8 from the cathode into the electrolyte started at this voltage stage.[15,46] As the cell continuously discharged to 2.13 V (blue star point), the peak intensity of Li_2S_x increased. It reached the maximum value when the voltage decreased to 2.08 V (purple star point), which verified that plenty of Li_2S_x released from the cathode into the electrolyte. In contrast, as for S@DICP, only a weak peak for Li_2S_x can be detected until the voltage reached down to 2.14 V (blue star point) and peak intensity only slightly increased in the whole discharge process. The results suggested that the DICP binder can confine the shuttle of lithium polysulfides more efficiently than that of PVdF and PAA.

To investigate the adsorption capability of lithium polysulfide with different binders, the same amount of Denka carbon black (CB), and different binder-CB composites (PVdF-CB, PAA-CB and DICP-CB) were added into the Li_2S_6-DME/DOL solution to compare the visual color changes. The color of the Li_2S_6-DME/DOL solution after 12h is shown in Figure S11 (Supporting Information). The Li_2S_6 solutions exposed to PVdF-CB and PAA-CB still exhibit

a typical orange color, which is similar to that of blank sample and solution with CB. In contrast, the solution exposed to the DICP-CB already becomes almost transparent, indicating strong adsorption of DICP to the lithium polysulfides. The strong adsorption capability of DICP to Li_2S_6 was further explored by using in-situ UV-vis spectroscopy. The absorption signal in the wavenumber range of 400-500 nm attributes to the Li_2S_6.[36,49] During the whole test period, the intensity signal of the Li_2S_6 solution exposed to DICP-CB composite shows a significantly higher decrease than that of PVdF-CB and PAA-CB. This suggested that DICP can be stronger than PVdF and PAA in adsorbing lithium polysulfides. Owing to the strong adsorption capability of DICP, the shuttle effect of lithium polysulfide is remarkably confined during battery cycling. As a result, the capacity maintains well even for a long term cycle.

Figure 5(d-f) show the X-ray photoelectron spectroscopy (XPS) analysis of the sulfur species formed on the surface of the corresponding lithium anode. After ten cycles, the surface of lithium anode is covered by a variety of sulfur species. In Figure 5(d), the peak at 169.3 is attributed to $TFSI^-$ anion. The S 2*p* peaks split into two peaks (S $2p_{3/2}$ and S $2p_{1/2}$) with a 2/1 intensity ratio and ~1.2 eV binding energy differences.[50] The small peak at lower binding energy of 167.3 eV can be assigned to the S(IV) degradation species of different sulfite salt, such as $Li_2(F_3CSO_2\text{-}N\text{-}SO_2)$, $LiSO_2CF_3$ or Li_2SO_3.[51,52] Another two components detected at lower binding energy of 163.8 eV (green) and 161.8 eV (orange) are ascribed to the bridging sulfur and terminal sulfur atoms of Li_2S_x, respectively.[50,53] Meanwhile, the signal of Li_2S is also observed at the binding energy of 160.5 eV, which is derived from the reduction of polysulfides into Li_2S at the surface of lithium anode.[53] The existence of lithium polysulfides on the surface lithium anode demonstrates that these species diffuse from the sulfur cathode toward the lithium anode, causing the capacity fading. The signal intensity of lithium polysulfides of S@DICP (Figure 5(f)) is lower than that of S@PVdF and S@PAA

(Figure 5(e)). This finding indicates high accordance with the previous results about in-situ XAS and in-situ UV-vis.

Density Functional Theory (DFT) calculation is utilized to simulate the confining capability for lithium polysulfides of different binders. Fragments of DICP, PEI, PAA, and PVdF are employed to represent the structures of the polymer binders in the modeling process (Figure 6(a)). Since only long-chain polysulfides are the most likely species to be dissolved in the electrolyte, Li_2S_8, Li_2S_6, and Li_2S_4 are chosen for this study. As shown in Figure 6(b), the DICP exhibits higher binding energy with polysulfides, indicating the existence of stronger strength between polysulfides and DICP, which is consistent with the results performed by in-situ XAS, in-situ UV-vis and XPS. In addition, the advantage of DICP is more conspicuous for longer chain polysulfides. The binding energy of DICP to Li_2S_8 can reach up to 1.32 eV, which is much higher than the value for PAA (1.01 eV) and PVdF (0.76 eV). Therefore, no Li_2S_8 can be detected from the in-situ XAS result of S@DICP when the cell discharges to 2.23 V.

3. Conclusion

With environment-friendly process, a novel DICP with multi-functional bonding groups as binder for Li-S batteries has been prepared through carboxy-amino ionic interaction. The crosslinked network of DICP binder can be readily dissolved in basic condition, enabling successful recycling of C-S composites from cycled Li-S cells with a simple washing method based on water. Besides, re-fabricated Li-S cells can deliver the discharge capacity at a similar level to fresh materials. Meanwhile, through effectively confining the dissolution of lithium polysulfides and maintain the integrity of electrode, the DICP binder enables a high sulfur loading electrode of 5.5 mg cm^{-2} with areal capacity of 6.39 mAh cm^{-2} while preserving stable cycling stability. Exploiting reversible crosslinked polymer binder for recyclable Li-S

batteries with high performance, this study provides an eco-efficient perspective for sustainable development of large-scale energy storage systems, a guidance that is pertinent to green chemistry and future circular economy.

4. Experimental Section

Details of materials and experimental procedures are listed in Supporting Information.

Supporting Information

Supporting Information is available from the Wiley Online Library or from the author.

Acknowledgements

Z.L. and X.H. contributed equally to this work. This work is funded by the Assistant Secretary for Energy Efficiency, the Office of Technology Transitions and Vehicle Technologies Office of the U.S. Department of Energy, under the Technoogy Commercialization (TCF) Fund projects and Advanced Battery Materials Research (BMR) Program. In-situ XAS was performed at the Advanced Light Source (ALS). Lawrence Berkeley National Laboratory (LBNL) is supported by the Director, Office of Science, Office of Basic Energy Sciences, of the US Department of Energy under contract no. DE-AC02-05CH11231. Z.L. acknowledges the support from the China Scholarship Council under Grant No. 201806240108. L.C.F and P.B.B gratefully acknowledge the supercomputer resources from the Texas A&M University High Performance Research Computing Center.

Received: ((will be filled in by the editorial staff))
Revised: ((will be filled in by the editorial staff))
Published online: ((will be filled in by the editorial staff))

References

[1] C. P. Grey, J. M. Tarascon, *Nat. Mater.* **2016**, *16*, 45.

[2] H. Xu, C. Peng, Y. Yan, F. Dong, H. Sun, J. Yang, S. Zheng, *Carbon Energy* **2019**, *1*, 276.

[3] G. Harper, R. Sommerville, E. Kendrick, L. Driscoll, P. Slater, R. Stolkin, A. Walton, P. Christensen, O. Heidrich, S. Lambert, A. Abbott, K. Ryder, L. Gaines, P. Anderson, *Nature* **2019**, *575*, 75.

[4] T. Or, S. W. D. Gourley, K. Kaliyappan, A. Yu, Z. Chen, *Carbon Energy* **2020**, *2*, 6.

[5] T. Keijer, V. Bakker, J. C. Slootweg, *Nat. Chem.* **2019**, *11*, 190.

[6] M. Jana, R. Xu, X.-B. Cheng, J. S. Yeon, J. M. Park, J.-Q. Huang, Q. Zhang, H. S. Park, *Energy Environ. Sci.* **2020**, *2*, *6*.

[7] L. Kong, B. Q. Li, H. J. Peng, R. Zhang, J. Xie, J. Q. Huang, Q. Zhang, *Adv. Energy Mater.* **2018**, *8*, 1800849.

[8] W. Shin, J. Lu, X. Ji, *Carbon Energy* **2019**, *1*, 165.

[9] H. Lin, L. Yang, X. Jiang, G. Li, T. Zhang, Q. Yao, G. W. Zheng, J. Y. Lee, *Energy Environ. Sci.* **2017**, *10*, 1476.

[10] Y. Chu, N. Chen, X. Cui, A. Liu, L. Zhen, Q. Pan, *J. Energy Chem.* **2020**, *46*, 99.

[11] L. Zhang, M. Ling, J. Feng, G. Liu, J. Guo, *Nano Energy* **2017**, *40*, 559.

[12] J. Song, M. L. Gordin, T. Xu, S. Chen, Z. Yu, H. Sohn, J. Lu, Y. Ren, Y. Duan, D. Wang, *Angew. Chemie* **2015**, *127*, 4399.

[13] Q. Zhang, H. Wan, G. Liu, Z. Ding, J. P. Mwizerwa, X. Yao, *Nano Energy* **2019**, *57*, 771.

[14] L. Du, Q. Wu, L. Yang, X. Wang, R. Che, Z. Lyu, W. Chen, X. Wang, Z. Hu, *Nano Energy* **2019**, *57*, 34.

[15] W. Chen, T. Lei, T. Qian, W. Lv, W. He, C. Wu, X. Liu, J. Liu, B. Chen, C. Yan, J. Xiong, *Adv. Energy Mater.* **2018**, *8*, 1702889.

[16] J. Liu, D. G. D. Galpaya, L. Yan, M. Sun, Z. Lin, C. Yan, C. Liang, S. Zhang, *Energy Environ. Sci.* **2017**, *10*, 750.

[17] X. Fu, L. Scudiero, W. H. Zhong, *J. Mater. Chem. A* **2019**, *7*, 1835.

[18] J. Liu, M. Sun, Q. Zhang, F. Dong, P. Kaghazchi, Y. Fang, S. Zhang, Z. Lin, *J. Mater. Chem. A* **2018**, *6*, 7382.

[19] F. Pei, T. H. An, J. Zang, X. J. Zhao, X. L. Fang, M. S. Zheng, Q. F. Dong, N. F. Zheng, *Adv. Energy Mater.* **2016**, *6*, 1502539.

[20] N. Akhtar, H. Shao, F. Ai, Y. Guan, Q. Peng, H. Zhang, W. Wang, A. Wang, B. Jiang, Y. Huang, *Electrochim. Acta* **2018**, *282*, 758.

[21] S. K. Park, J. K. Lee, Y. C. Kang, *Adv. Funct. Mater.* **2018**, *28*, 1705264.

[22] S. K. Park, J. Lee, T. Hwang, B. Jang, Y. Piao, *ACS Appl. Mater. Interfaces* **2017**, *9*, 2430.

[23] C. Ye, L. Zhang, C. Guo, D. Li, A. Vasileff, H. Wang, S. Z. Qiao, *Adv. Funct. Mater.* **2017**, *27*, 1702524.

[24] Y. Shi, G. Liu, R. Jin, H. Xu, Q. Wang, S. Gao, *Carbon Energy* **2019**, *1*, 253.

[25] J. Cosmidis, A. S. Templeton, *Nat. Commun.* **2016**, *7*.

[26] J. Ren, Y. Huang, H. Zhu, B. Zhang, H. Zhu, S. Shen, G. Tan, F. Wu, H. He, S. Lan, X. Xia, Q. Liu, *Carbon Energy,* DOI: 10.1002/cey2.44.

[27] S. Zhou, C. Fang, X. Song, G. Liu, *Carbon Energy* **2020**, *2*, 143.

[28] H. Yuan, J. Q. Huang, H. J. Peng, M. M. Titirici, R. Xiang, R. Chen, Q. Liu, Q. Zhang, *Adv. Energy Mater.* **2018**, *8*, 1802107.

[29] Y. Jiao, W. Chen, T. Lei, L. Dai, B. Chen, C. Wu, J. Xiong, *Nanoscale Res. Lett.* **2017**, *12*, 195.

[30] Q. Guo, Z. Zheng, *Adv. Funct. Mater.* **2020**, *30*, 1907931.

[31] H. Chen, M. Ling, L. Hencz, H. Y. Ling, G. Li, Z. Lin, G. Liu, S. Zhang, *Chem. Rev.* **2018**, *118*, 8936.

[32] Q. Qi, X. Lv, W. Lv, Q. H. Yang, *J. Energy Chem.* **2019**, *39*, 88.

[33] X. Liu, T. Qian, J. Liu, J. Tian, L. Zhang, C. Yan, *Small* **2018**, *14*, 1801536.

[34] H. Ye, D. Lei, L. Shen, B. Ni, B. Li, F. Kang, Y. B. He, *Chinese Chem. Lett.* **2020**, *31*, 570.

[35] H. Zhang, X. Hu, Y. Zhang, S. Wang, F. Xin, X. Chen, D. Yu, *Energy Storage Mater.* **2019**, *17*, 293.

[36] W. Chen, T. Qian, J. Xiong, N. Xu, X. Liu, J. Liu, J. Zhou, X. Shen, T. Yang, Y. Chen, C. Yan, *Adv. Mater.* **2017**, *29*, 1605160.

[37] Q. Pang, X. Liang, C. Y. Kwok, J. Kulisch, L. F. Nazar, *Adv. Energy Mater.* **2017**, *7*, 1601630.

[38] A. Kasprzak, M. Popławska, M. Bystrzejewski, O. Łabędź, I. P. Grudziński, *RSC Adv.* **2015**, *5*, 85556.

[39] Z. Xu, J. Yang, T. Zhang, Y. Nuli, J. Wang, S. ichi Hirano, *Joule* **2018**, *2*, 950.

[40] M. H. Ahmed, J. A. Byrne, J. A. D. McLaughlin, A. Elhissi, W. Ahmed, *Appl. Surf. Sci.* **2013**, *273*, 507.

[41] G. Zhang, Y. Yang, Y. Chen, J. Huang, T. Zhang, H. Zeng, C. Wang, G. Liu, Y. Deng, *Small* **2018**, *14*, 1801189.

[42] M. Li, J. Zhou, J. Zhou, C. Guo, Y. Han, Y. Zhu, G. Wang, Y. Qian, *Mater. Res. Bull.* **2017**, *96*, 509.

[43] H. J. Peng, G. Zhang, X. Chen, Z. W. Zhang, W. T. Xu, J. Q. Huang, Q. Zhang, *Angew. Chemie - Int. Ed.* **2016**, *55*, 12990.

[44] T. Z. Hou, W. T. Xu, X. Chen, H. J. Peng, J. Q. Huang, Q. Zhang, *Angew. Chemie - Int. Ed.* **2017**, *56*, 8178.

[45] A. Bhargav, J. He, A. Gupta, A. Manthiram, *Joule* **2020**, *4*, 285.

[46] M. Cuisinier, P. E. Cabelguen, S. Evers, G. He, M. Kolbeck, A. Garsuch, T. Bolin, M. Balasubramanian, L. F. Nazar, *J. Phys. Chem. Lett.* **2013**, *4*, 3227.

[47] X. Yang, X. Gao, Q. Sun, S. P. Jand, Y. Yu, Y. Zhao, X. Li, K. Adair, L. Y. Kuo, J. Rohrer, J. Liang, X. Lin, M. N. Banis, Y. Hu, H. Zhang, X. Li, R. Li, H. Zhang, P. Kaghazchi, T. K. Sham, X. Sun, *Adv. Mater.* **2019**, *31*, 1901220.

[48] M. Ling, L. Zhang, T. Zheng, J. Feng, J. Guo, L. Mai, G. Liu, *Nano Energy* **2017**, *38*, 82.

[49] J. Song, Z. Yu, M. L. Gordin, D. Wang, *Nano Lett.* **2016**, *16*, 864.

[50] M. Baloch, A. Vizintin, R. K. Chellappan, J. Moskon, D. Shanmukaraj, R. Dedryvère, T. Rojo, R. Dominko, *J. Electrochem. Soc.* **2016**, *163*, A2390.

[51] C. Xu, B. Sun, T. Gustafsson, K. Edström, D. Brandell, M. Hahlin, *J. Mater. Chem. A* **2014**, *2*, 7256.

[52] D. Aurbach, E. Pollak, R. Elazari, G. Salitra, C. S. Kelley, J. Affinito, *J. Electrochem. Soc.* **2009**, *156*, A694.

[53] C. Zu, Y. Fu, A. Manthiram, *J. Mater. Chem. A* **2013**, *1*, 10362.

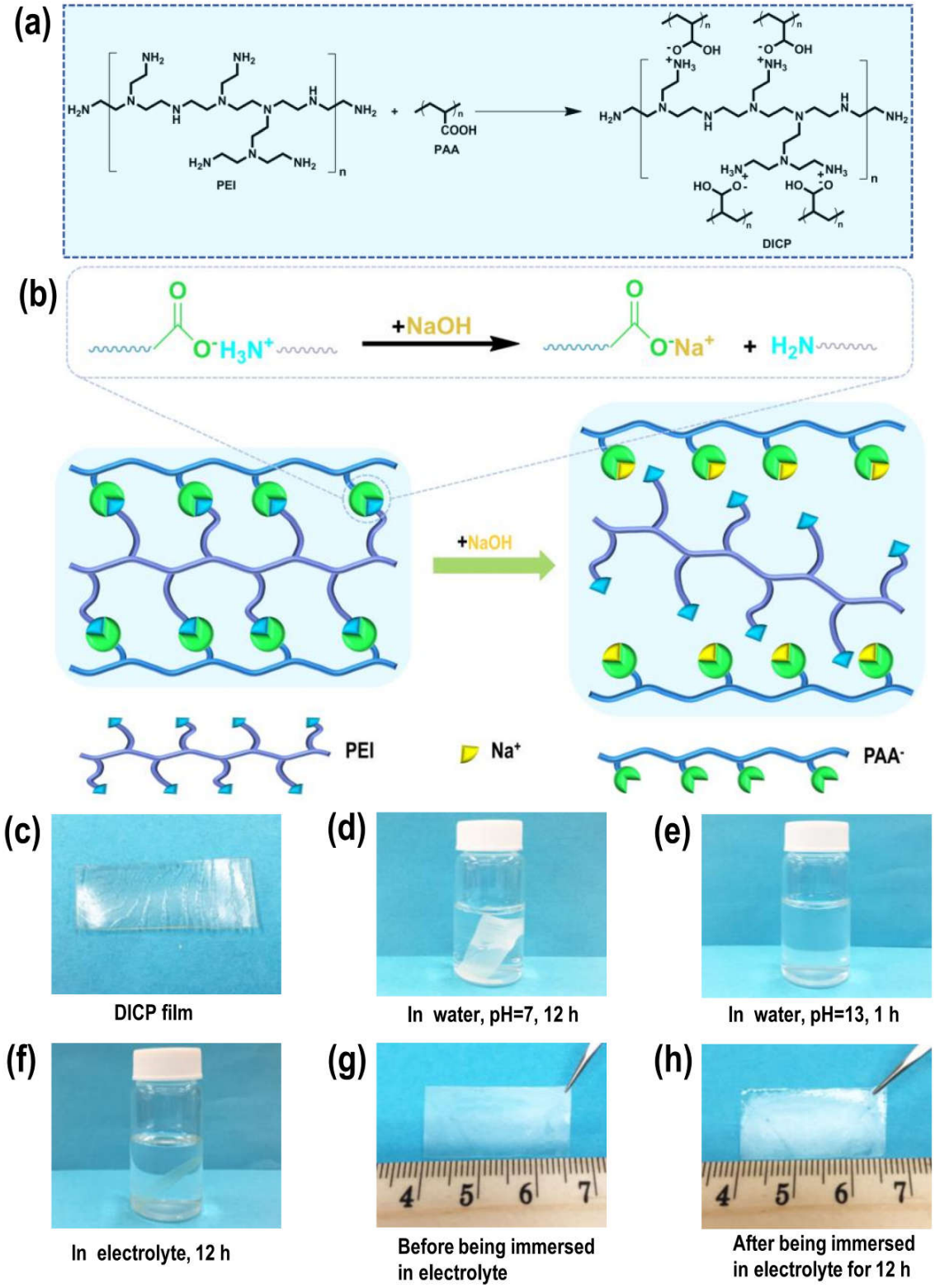

Figure 1. (a) Synthesis scheme of DICP through carboxy-amino ionic interaction between PAA and PEI; (b) Schematic diagram of DICP dissociated in the aqueous sodium

hydroxide; (c) Photograph of DICP film; (d) and (e) Photographs of DICP film immersed in distilled water (pH=7) for 12h and basic aqueous solution (pH=13) for 1h, respectively; (f) Photograph of DICP film immersed in an electrolyte (1.0 M LiTFSI in 1:1(v/v) DOL/DME containing 1 wt% $LiNO_3$) for 12h; (g) and (h) Photograph respectively shows the size of DICP film before and after being immersed in electrolyte for 12h.

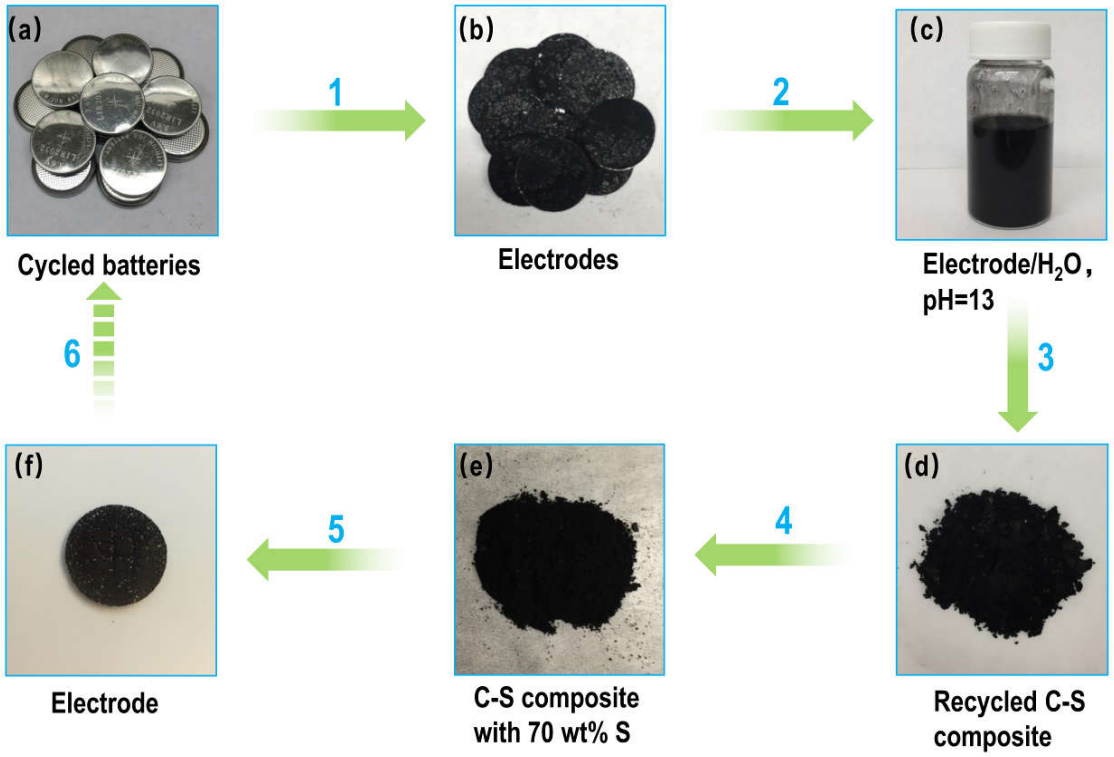

Figure 2. Photographs illustrating the recycling processes of cycled Li-S batteries (a) Coin cell of Li-S batteries after 100 cycles at 0.1C; (b) Sulfur electrodes obtained from cycled Li-S batteries; (c) Dispersed electrode materials in alkaline water (pH=13); (d) Recycled C-S composite obtained after washing (with distilled water)-centrifugation-drying. (e) Refilled C-S composite with 70 wt% sulfur content. (f) Reproduced sulfur electrode with sulfur loading of 5.5 mg cm^{-2}.

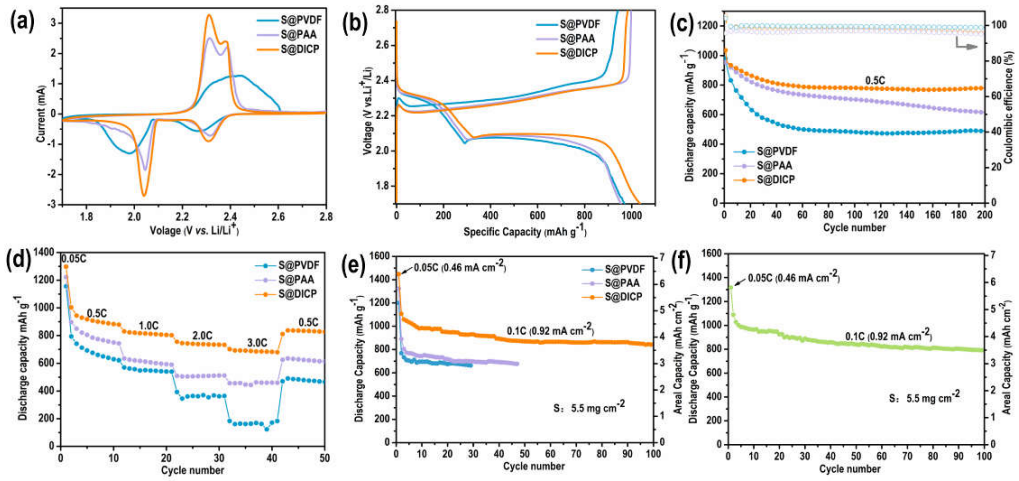

Figure 3 (a) CV curves of sulfur electrodes with different binders at a scan rate of 0.1 mV s^{-1} over the potential range of 1.7-2.8 V vs. Li/Li^+; (b) discharge-charge curves of sulfur electrodes with different binders at 0.5C; (c) Cycling performance of sulfur cathodes with different binders at current density of 0.5C, sulfur loading 1.0 mg cm^{-2} on aluminum foil; (d) Rate performance of sulfur electrodes with different binders, sulfur loading 1.0 mg cm^{-2} on aluminum foil; (e) Cycling performance of sulfur cathodes with different binder, sulfur loading of 5.5 mg cm^{-2} on nickel foam; (f) Cycling performance of sulfur cathode prepared from recycled carbon materials, with sulfur loading of 5.5 mg cm^{-2} on nickel foam.

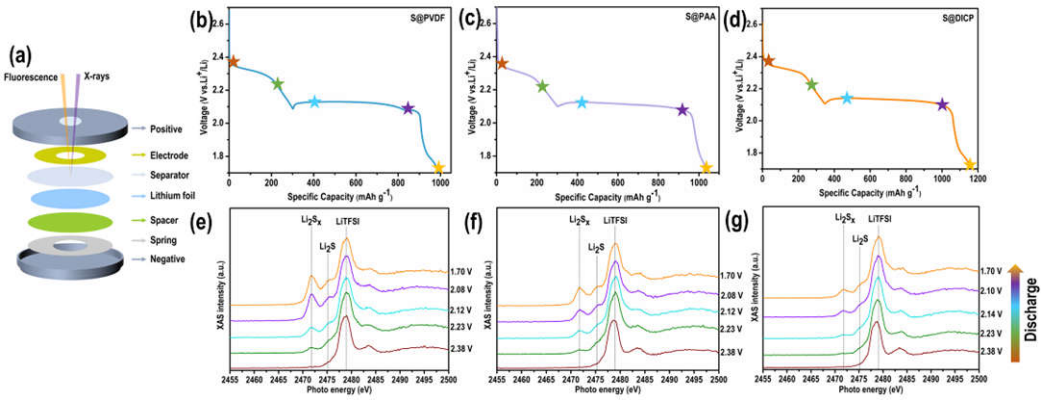

Figure 4. (a) Schematic of the in-situ XAS experiment set-up; (b), (c), and (d) Discharge curve of in-situ batteries for S@PVdF, S@PAA, and S@DICP, respectively. (e), (f) and (g) Selected in-situ XAS curves of S@PVdF, S@PAA, and S@DICP cathodes, respectively.

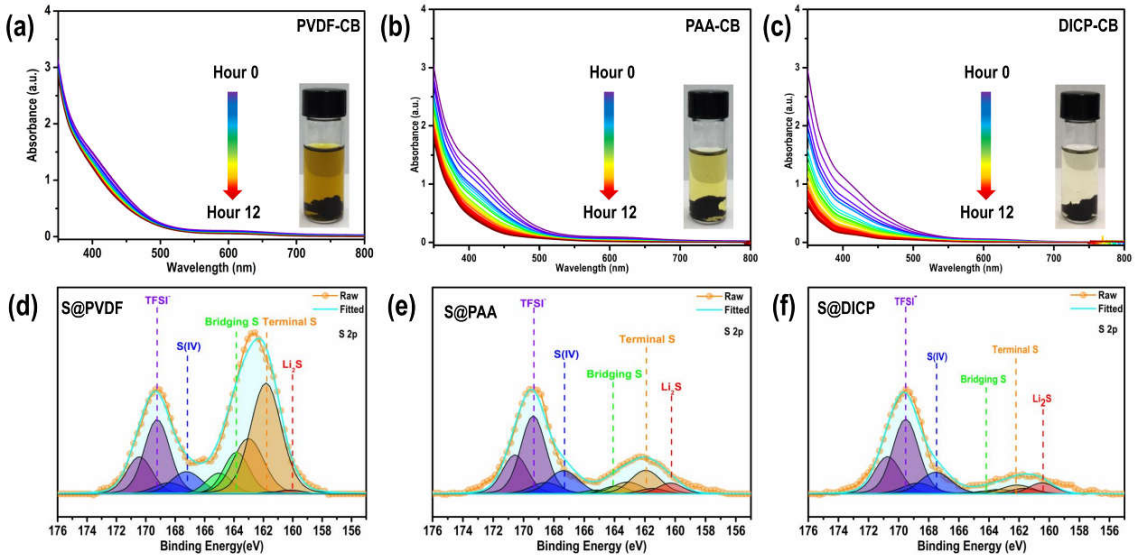

Figure 5. a-c) In-situ UV–vis absorbance spectra of the Li_2S_6-DME/DOL solutions after exposure to the different binder absorbers (PVdF-CB, PAA-CB and DICP-CB composite). Inserted photo is the vial of Li_2S_6-DME/DOL solution after exposure to the solution with corresponding binder absorber for 12h. XPS S 2p spectra of lithium anode obtained after 10 cycles at 0.1 C: d-f) corresponding to the sulfur cathode using PVdF, PAA, and DICP as binder, respectively.

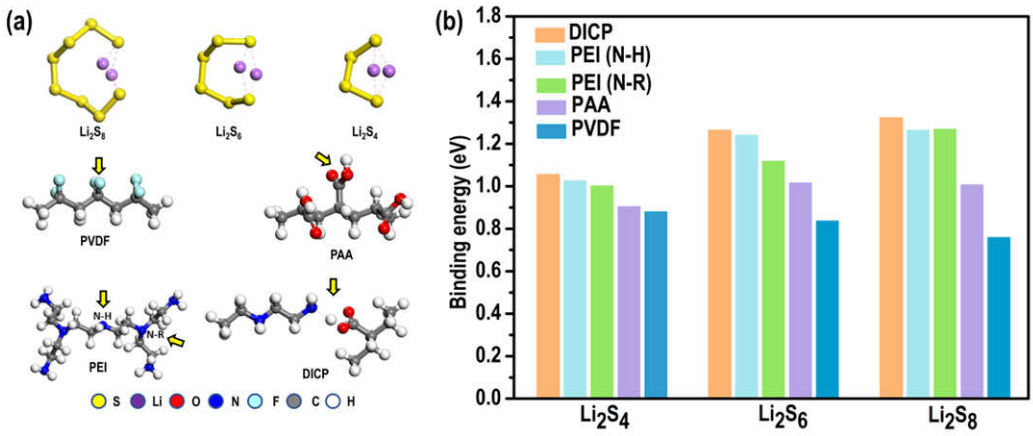

Figure 6. (a) Optimized structures of lithium polysulfides (Li_2S_8, Li_2S_6, and Li_2S_4) and polymer fragments (PVdF, PAA, PEI, and DICP). Arrows indicate the site/functional group where the polysulfides are initially placed to calculate their corresponding binding energies. (b) Calculated binding energies of lithium polysulfides (Li_2S_8, Li_2S_6, and Li_2S_4) with different polymer fragments in DME.

A reversible crosslinked polymer was employed as a binder for Li-S batteries with high sulfur loading. The crosslinked binder can be easily dissolved in basic solution, providing a facile strategy to recycle the carbon/sulfur composite through a simple washing method based on water. This study provides new guidance for combining large-scale energy storage systems with sustainability.

Keyword: binder; recyclable; high sulfur loading; lithium sulfur batteries

Zhimeng Liu, Xin He, Chen Fang, Luis E. Camacho-Forero, Yangzhi Zhao, Yanbao Fu, Jun Feng, Robert Kostecki, Perla B. Balbuena, Junhua Zhang, Jingxin Lei and Gao Liu*

Reversible crosslinked polymer binder for recyclable lithium sulfur batteries with high performance